DOI: 10.13009/EUCASS2025-048
11TH EUROPEAN CONFERENCE FOR AERONAUTICS AND SPACE SCIENCES (EUCASS)

Low-Altitude Flight Test of 30m Wingspan Stratospheric UAV EAV-4

*Hyoung Sik Choi**†, Sung-Yug Kim, Seungchan Shin, Yeondeuk Jung, Hyeok Ryu and Yung Gyo Lee**
** Korea Aerospace Research Institute,*
Deajeon, Republic of Korea
chs@kari.re.kr – kkisy@kari.re.kr
† Corresponding Author

Abstract
The Korea Aerospace Research Institute (KARI) is developing the EAV-4, a solar-powered stratospheric unmanned aerial vehicle (UAV) designed for high-altitude, long-endurance missions. Building upon experience from previous models such as the EAV-3, which demonstrated successful high-altitude and long-duration flights, the EAV-4 features an extended wingspan of 30 meters, dual-redundant flight control systems, and a payload capacity of 20 kg. This paper presents the design methodology, focusing on aerodynamic optimization, structural flexibility, and fault-tolerant control systems. A series of low-altitude flight tests were conducted to validate the aircraft's control performance under various flight modes, including attitude, velocity, and altitude hold. Simulation and hardware-in-the-loop testing were employed to refine the flight control system, while structural analyses accounted for flexible-body effects and the added mass effect. The results confirm stable flight characteristics within the target speed range (20–30 km/h) and highlight the UAV's potential for future long-endurance stratospheric operations.

1. Introduction

The Korea Aerospace Research Institute (KARI) has been developing a stratospheric UAV for high-altitude, long-endurance operations. The stratospheric UAV developed by KARI is powered by two electrically driven propellers. It utilizes solar panels for in-flight energy harvesting during daytime operations, while onboard batteries provide power during nighttime, enabling continuous flight until sunrise [1].
The development of the stratospheric UAV has progressed through several stages [2,3], and the current model, the EAV-4, has a wingspan of 30 meters. Previous flight test records include the EAV-3, which conducted high-altitude tests at 14.1 km in 2015 [4], 18.5 km in 2016, and 17 km in 2019, and a 53-hour endurance flight in 2020 [5–8].
Figure 1 presents an image captured during the 18.5 km altitude flight conducted on August 12, 2016. The image demonstrates the UAV's capability for ground observation applications.



Figure 1: EAV-3 High Altitude Test (18.5km) On-board Image (Left) and Look-Down Image (Right)

Copyright © 2025 by First Author. Posted online by the EUCASS association with permission.

DOI: 10.13009/EUCASS2025-048

Table 1 summarizes the key performance specifications of the stratospheric UAV currently under development by the Korea Aerospace Research Institute (KARI). As indicated, the EAV-4 model has been designed with a payload capacity of 20 kg, which necessitated substantial increases in both the maximum takeoff weight and wingspan. The EAV-4 remains in the development phase, and this paper presents the results of recent low-altitude flight tests conducted to validate its performance and flight control systems.

Table 1: EAV Series Specifications

	EAV-2H+	**EAV-3**	**EAV-4**
Weight [kg]	21	53	150 (payload 20kg)
Speed(EAS) [km/h]	35-45	30-40	20-30
Wing Span [m]	11	20	30
Redundancy [-]	Single	Dual	Dual, standby
Altitude Record [km]	5, 10	14.1, 18.5	Test flight

2. Design of Aircraft

The airframe configuration of the EAV-4 was developed based on the accumulated experience from the EAV-3, adopting a similar overall design. Through iterative refinement of both aerodynamic shape and structural layout, the final form of the EAV-4i was derived. Given the characteristics of stratospheric UAVs—which include low-speed flight and a high aspect ratio—the resulting configuration inherently exhibits reduced controllability compared to conventional rigid-body aircraft. To address this, the incorporation of wing dihedral was deemed necessary to enhance lateral stability.

The power system consists of solar cells and rechargeable batteries. The propeller, driven by an electric motor, was designed with a focus on high efficiency. Both the motor and the inverter used in the propulsion system are domestically developed components, realized through this project.

The flight control system (FCS) features a dual-redundant architecture to ensure reliability, and the actuators are similarly implemented with dual redundancy. In addition, the control surfaces are segmented to allow for fault-tolerant operation in the event of a control surface failure.

To accommodate this segmentation, the horizontal stabilizer was redesigned from an all-moving T-tail to a hinged inverted T-tail configuration.

The developed airframe configuration is shown in Figure 2.

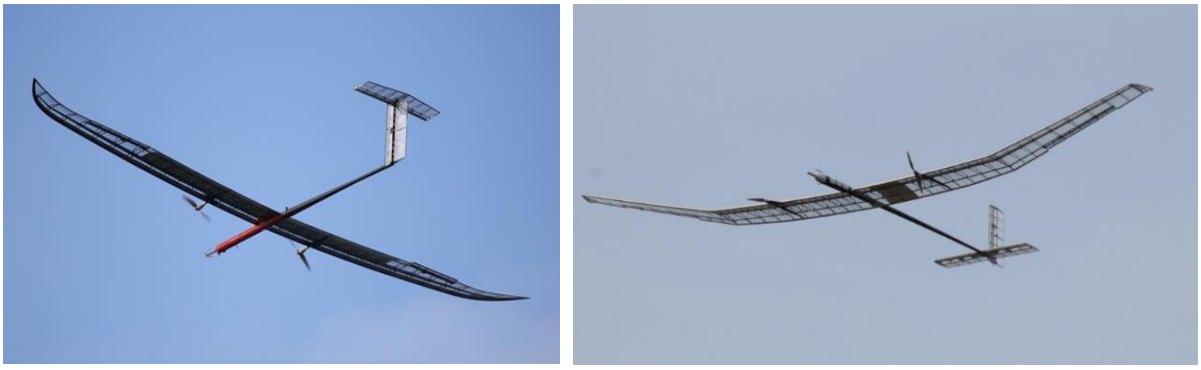


Figure 2: Solar Powered EAV-3 (Left) and EAV-4 (Right)

DOI: 10.13009/EUCASS2025-048

The aerodynamics team conducted propeller optimization design and testing, and performed CFD analysis to derive the final airframe shape. The air data measurement system provides information on velocity, angle of attack, and sideslip angle. The air data system (ADS) consists of one five-hole probe and two Pitot tubes, and outputs calculated based on averaged sensor values. The five-hole sensor was calibrated for velocity, angle of attack, and sideslip angle through wind tunnel experiments.

Figure 3 presents the CFD analysis that accounts for segmented control surfaces during the shape design process, as well as the wind tunnel testing of the five-hole air data system.

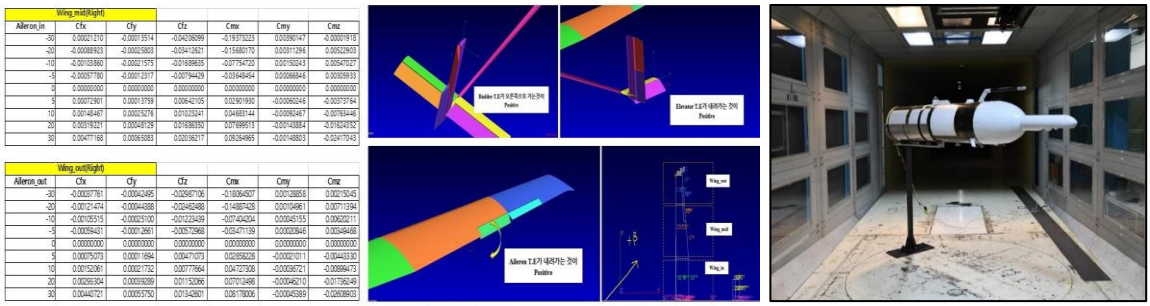


Figure 3: CFD Aerodynamic Analysis (Left) and ADS Wind Tunnel Test (Right)

The structural team conducted both static load and dynamic flutter analyses based on the finalized airframe design, and validated the results through ground testing, as shown in Figure 4 (left). The flutter analysis revealed that the aircraft enters a critical risk regime at speeds exceeding approximately 35 km/h. Therefore, the flight control system must be carefully managed to prevent operations beyond this threshold.

Another notable characteristic of this UAV is its flexible structural behavior. Unlike conventional rigid-body aircraft, where control authority generally increases with airspeed, the analysis indicated that for this flexible platform, control authority begins to deteriorate beyond a specific speed threshold. Figure 4 (right) presents the analysis results illustrating this degradation phenomenon.

Figure 5 presents a comparison table between the vibration test results and the analytical predictions, demonstrating good agreement between the experimental and analytical data.

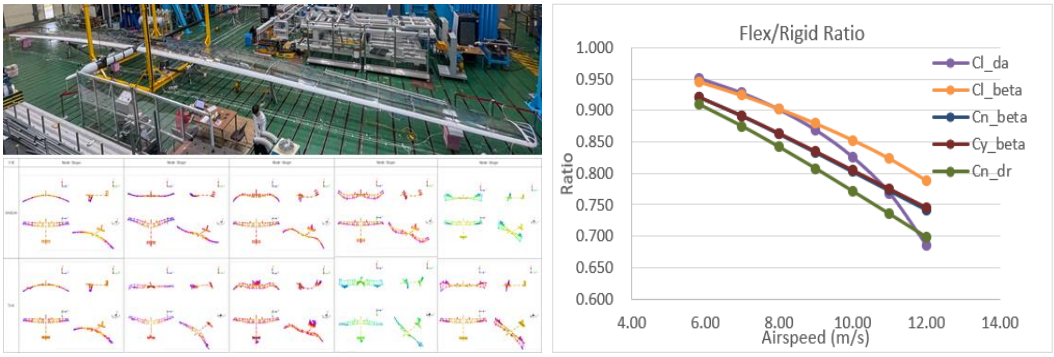


Figure 4: Ground Vibration Test (Left) and Control Degradation with Increasing Airspeed (Right)

Index	Mode Description (Primary + Secondary)	Symmetry	Test	Analysis (with VFM+Sensor Mass)	
			Freq [Hz]	Freq [Hz]	% Error
7	MW 1VB	Sym	0.69	0.65	5.8%
13	MW_LB1+MW_VB2	Sym	3.64	3.69	-1.4%
14	MW_VB2+Boom_VB2	Sym	2.89	3.06	-5.9%
15	MW_T+MW_VB2	Sym	4.45	4.06	8.8%
29	MW_T+Aileron	Sym	6.22	6.44	-3.6%

Figure 5: Comparison Between Vibration Analysis and Test Results

DOI: 10.13009/EUCASS2025-048

Additionally, since the aircraft is lightweight and features a surface made of Mylar material, the structural analysis software accounts for the added mass effect [9]. This effect results in an increase in the inertia moment, which varies depending on altitude.

Figure 6 presents the analysis results of the added mass (virtual mass) as a function of altitude.

❑ **Altitude 0 km (rho = 1.225 kg/m³)**

Inertia Properties	Dry (A)	Wet (B)	% (B/A)
X-directional Mass	152.1	162.6	107%
Y-directional Mass	152.1	155.9	103%
Z-directional Mass	152.1	275.2	181%
XCG (Y-directional Mass)	3446.6	3647.0	106%
XCG (Z-directional Mass)	3446.6	3694.1	107%
YCG (X-directional Mass)	0.9	0.8	89%
YCG (Z-directional Mass)	0.9	1.3	135%
ZCG (X-directional Mass)	8.6	47.6	556%
ZCG (Y-directional Mass)	8.6	-12.8	-150%
Ixx about CG	2.77E+09	8.68E+09	314%
Iyy about CG	1.33E+09	1.84E+09	138%
Izz about CG	4.09E+09	4.96E+09	121%

❑ **Altitude 10 km (rho = 0.4135 kg/m³)**

Inertia Properties	Dry (A)	Wet (B)	% (B/A)
X-directional Mass	152.1	155.6	102%
Y-directional Mass	152.1	153.4	101%
Z-directional Mass	152.1	193.7	127%
XCG (Y-directional Mass)	3446.6	3515.0	102%
XCG (Z-directional Mass)	3446.6	3565.1	103%
YCG (X-directional Mass)	0.9	0.9	96%
YCG (Z-directional Mass)	0.9	1.1	117%
ZCG (X-directional Mass)	8.6	53.4	625%
ZCG (Y-directional Mass)	8.6	32.8	383%
Ixx about CG	2.77E+09	4.77E+09	172%
Iyy about CG	1.33E+09	1.51E+09	113%
Izz about CG	4.09E+09	4.39E+09	107%

❑ **Altitude 20 km (rho = 0.08891 kg/m³)**

Inertia Properties	Dry (A)	Wet (B)	% (B/A)
X-directional Mass	152.1	152.9	100%
Y-directional Mass	152.1	152.4	100%
Z-directional Mass	152.1	161.0	106%
XCG (Y-directional Mass)	3446.6	3461.4	100%
XCG (Z-directional Mass)	3446.6	3477.3	101%
YCG (X-directional Mass)	0.9	0.9	99%
YCG (Z-directional Mass)	0.9	1.0	104%
ZCG (X-directional Mass)	8.6	4.8	56%
ZCG (Y-directional Mass)	8.6	3.2	37%
Ixx about CG	2.77E+09	3.20E+09	115%
Iyy about CG	1.33E+09	1.37E+09	103%
Izz about CG	4.09E+09	4.16E+09	102%

Figure 6: Nominal (Dry case) and Added Mass (Wet case)

3. Flight Control System

In flight dynamics modeling, the aerodynamic data were primarily based on a parameterized DATCOM aerodynamic database, which was further refined by incorporating results from CFD aerodynamic analyses. Propeller modeling was performed using a Blade Element Momentum Theory (BEMT) approach, while the motor inverter model employed a simple delay representation. Structural flexibility was accounted for by incorporating the control effectiveness characteristics previously calculated in Figure 4, and the model was implemented to allow variations in the moments of inertia.

The six-degree-of-freedom flight dynamics model was utilized in ground simulation tests to validate the flight control system. Additionally, a ground reaction model was included to support takeoff and landing training.

Figure 7 illustrates the ground integrated test setup.

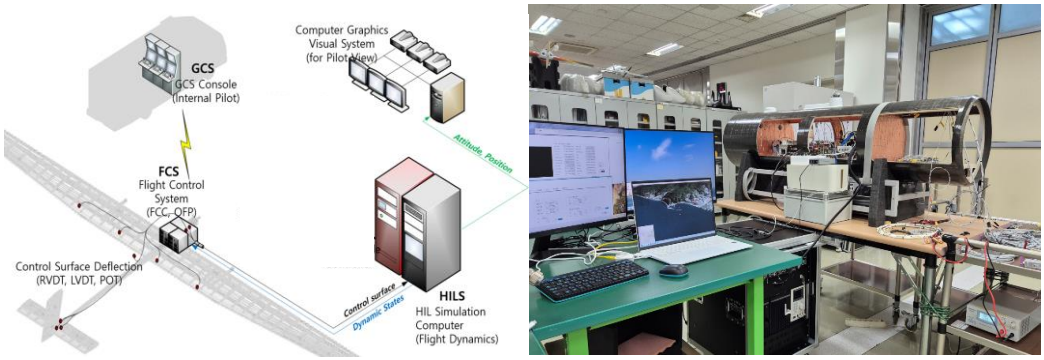


Figure 7: Hardware-In-the-Loop Concept (Left) and Test-Bench (Right)

However, due to the challenges associated with operating a large-scale aircraft, a scaled-down model was utilized to verify the flight control system. Tests were conducted to validate the system under various conditions, including control surface displacement limits to simulate actuator failures and rearward shifts of the center of gravity to account for uncertainties in weight distribution. The flight control system was thus verified in advance using these simulations.

The same flight control laws as those applied to the full-scale aircraft were implemented. These control laws were developed in MATLAB and subsequently converted into auto-generated code for deployment.

DOI: 10.13009/EUCASS2025-048

Since this aircraft operates at low speeds, it is necessary to monitor wind conditions. Therefore, a wind measurement instrument, as shown in Figure 8, was developed and utilized. This device enables estimation of the wind field. The wind measurement equations are as follows [4]:

Equation (1) represents the magnitude of the incoming wind, and Equation (2) indicates the direction of the incoming wind. The notation used in these equations can be referenced in Figure 8.

$$W_h = \sqrt{U_a{}^2 + V_g{}^2 - 2U_a V_g \cos(\psi_u - \psi_v)} \tag{1}$$

$$\psi_w^{from} = \tan^{-1}\frac{W_E^{from}}{W_N^{from}} = \tan^{-1}\left(\frac{U_a \sin\psi_u - V_g \sin\psi_v}{U_a \cos\psi_u - V_g \cos\psi_v}\right) \tag{2}$$

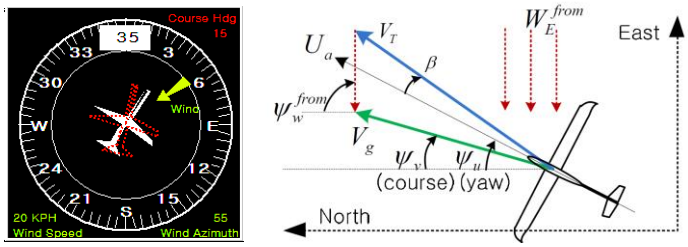


Figure 8: Wind Measurement Instrument (Left) and Geometry (Right)

4. Flight Test and Results

Figure 9 shows an overview of the low-altitude flight test conducted at the Goheung Flight Test Center, located in the southern region of South Korea [10].
A vehicle-mounted local ground control station (GCS), installed at the Goheung test site, is used for takeoff and landing operations. Meanwhile, a remote GCS located at the KARI headquarters in Daejeon supports high-altitude and long-range missions. The local and remote GCS are interconnected via an Ethernet link, allowing seamless switching depending on the operational phase and mission requirements. Communication between the GCS and the UAV is performed via a C2 data link.

For aircraft takeoff, an electric cart is employed to ensure safe and controlled liftoff. Landing is performed using skid-type gear without any additional landing apparatus.



Figure 9: EAV-4 GCS (Left) and Low Altitude Flight Test (Right)

Figure 10 presents the flight test result graphs from the low-altitude test conducted on April 27, 2025. Tests were performed in attitude hold mode (ATT mode) as well as velocity and altitude hold modes (V and H modes). The altitude control is achieved through thrust adjustments, while speed control is managed via pitch attitude. Turns are primarily controlled using the rudder.

Figure 10 (left) shows the attitude hold mode response graph, and Figure 10 (right) displays the velocity and altitude response graphs.

DOI: 10.13009/EUCASS2025-048

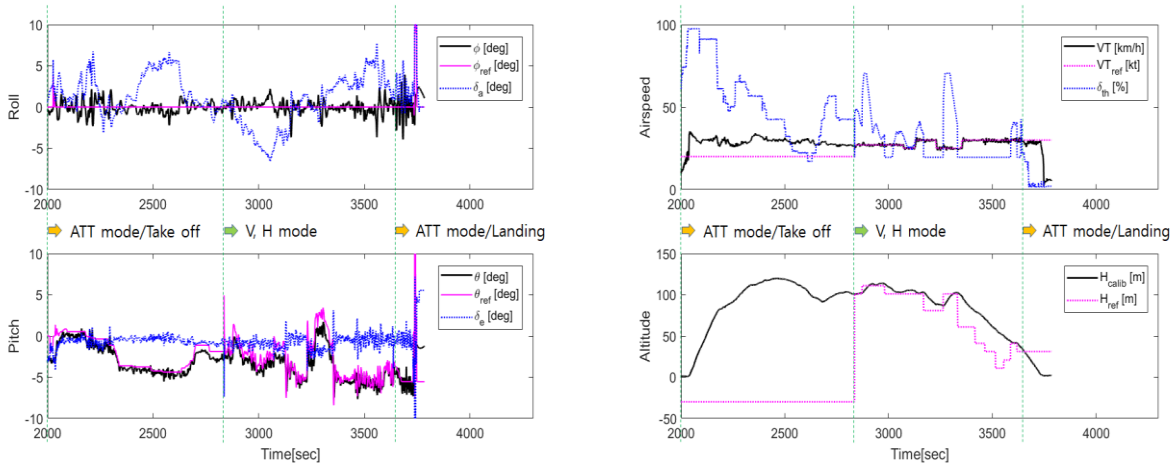


Figure 10: Attitude Response(left) and Airspeed/Altitude Response(right)

Figure 10 demonstrates that the aircraft accurately follows the commanded attitude, velocity, and altitude. Takeoff occurred around 2000 seconds in attitude hold mode (ATT mode), followed by testing in altitude and velocity hold modes (V and H modes), before returning to attitude hold mode for landing.

In this flight test, the flight speed range was set between 24 km/h and approximately 30 km/h. For future flights, the speed range will be adjusted to 20 km/h to 30 km/h for further testing.

The test program is progressively expanding to include automatic heading hold mode and automatic climb/descent guidance mode. Concurrently, various other tests are underway, such as low-temperature and low-pressure chamber tests as well as long-duration endurance tests. The ultimate goal is to achieve a continuous long-endurance flight of 30 days at high altitude.

References

[1] Oh, S., Kim, J-Y., Yu, G., “Technical Challenges of Stratospheric Solar Drones”, SASE 2024 Spring Conference (Korean).
[2] Ahn, S. M., Hwang, S. J., Lee, Y. G., Kim, C., “Development of Electrical Air Vehicle for Long Endurance”, 2013 Asia-Pacific International Symposium on Aerospace Technology Conference.
[3] Hwang, S., Kim, S., Kim, C., Lee, Y. G., “Aerodynamic Design of the Solar-Powered High Altitude Long Endurance (HALE) Unmanned Aerial Vehicle (UAV)”, 17(2016), IJASS, pp.132.
[4] Choi, H. S., Jung Y. D., Ahn, S. M., Ryu, H., Kim, S. Y., Kim, S. H., “Flight Test of HALE UAV and Airborne Wind Measurement”, 2016 Asia-Pacific International Symposium on Aerospace Technology Conference.
[5] Ahn, S. M., Kim, S. Y., Choi, H. S., Ryu, H., Kim, S. H., “Analysis of the Flight Test Data of HLE Solar Powered UAV EAV-3”, KSAS 2016 Fall Conference (Korean).
[6] Choi, H. S., Jung Y. D., Kim, S. Y., Ahn, S. M., Ryu, H., “17 km Flight Test Results of Solar HALE UAV EAV-3x”, KSAS 2019 Fall Conference (Korean).
[7] Hwang, S., “Stratosphere Solar-Powered UAV’s Long Endurance Flight Test”, KSAS 2020 Fall Conference (Korean).
[8] Park, P., Lee, B., L, Y. G., Hwang, S., “53 Hour Flight Test of Stratospheric Solar HALE UAV”, KSPE 2020 Fall Conference (Korean).
[9] https://en.wikipedia.org/wiki/Added_mass, Wikipedia.
[10] https://youtu.be/ldOwltk5Lv0?si=KD2p05COSW0X6fii, KARI TV.